What the mismatch between current geodetic data and paleoseismic data in southern Cascadia can tell us about the earthquake cycle?

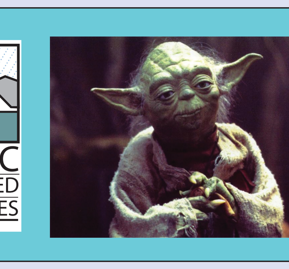

Jason “Jay” R. Patton [1,2]

Tom H. Leroy [2,3]

1. CEOAS, Oregon State University, Corvallis, OR, United States.
2. Cascadia GeoSciences, Bayside, CA, United States.
3. Pacific Watershed Associates, McKinleyville, CA, United States

http://earthjay.com
http://cascadiageo.org
http://pacificwatershed.com

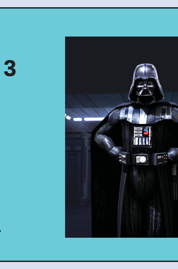

Interseismic vertical deformation in northern California is collocated with paleoseismic evidence of coseismic vertical deformation, but they are not opposite in sense of motion as expected with the classic subduction zone model as evidenced from Plafker's work on the 1960 Chile and 1964 Alaska subduction zone earthquakes.

GPS and tide-gage data are compared with paleoseismic data in the form of sediment cores in the region of Humboldt Bay and Crescent City, northern California. In Humboldt Bay, North Spit (NOAA) and Mad River slough (campaign) tide gage data show rates of subsidence of ~3 and ~2 mm/yr respectively, while the Crescent City tide gage (NOAA) shows ~3mm/yr of emergence. GPS vertical motion rates show a similar gradient of subsidence and uplift in this region, consistent with the tide gage data. Paleoecologic estimates of the magnitude of coseismic subsidence in Mad River slough are ~0.5 m.

Tectonic deformation at the Cascadia subduction zone:

Cascadia subduction zone

Nelson, et al., 2004
Chaytor, et al., 2004

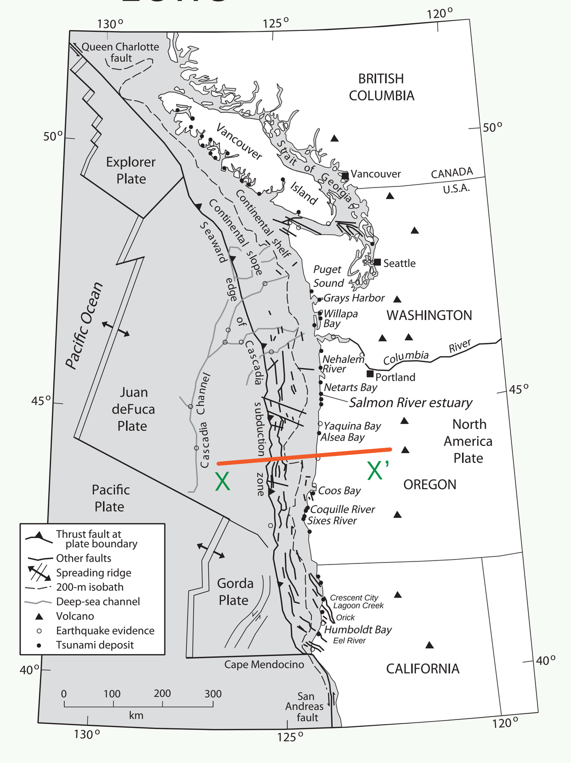

Plate configuration for the Cascadia subduction zone (CSZ). Juan de Fuca and Gorda plates are subducting northeastwardly oblique beneath the North America plate at ~36 mm/yr in the Humboldt Bay region. Paleoseismic core sites (marine and terrestrial) are plotted as circles.

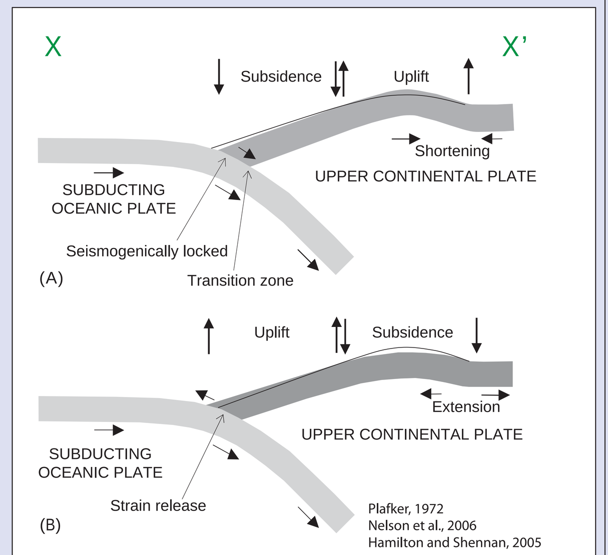

Schematic diagrams showing the pattern of (A) inter-seismic and (B) co-seismic deformation associated witha subduction zone earthquake during an earthquake deformation cycle. Adapted from Plafker (1972) to reflect the spatial pattern of tectonic deformation during the earthquake cycle in Cascadia.

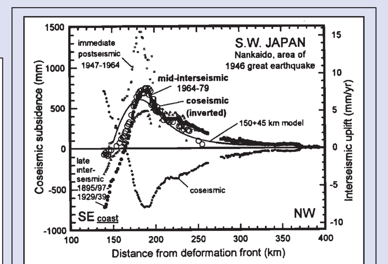

Hyndman & Wang, 1995

Repeated leveling results across the Nankai margin of southwestern Japan giving the coseismic subsidence (small solid dots), coseismic subsidence inverted (large solid dots), and the interseismic uplift rate for three intervals. The interseismic vertical axis is scaled relative to the coseismic axis by time interval between great earthquakes. Note the agreement in the location of the peaks for the coseismic (inverted) and interseismic profiles, especially for the mid-interseismic period.

Wang et al., 2003

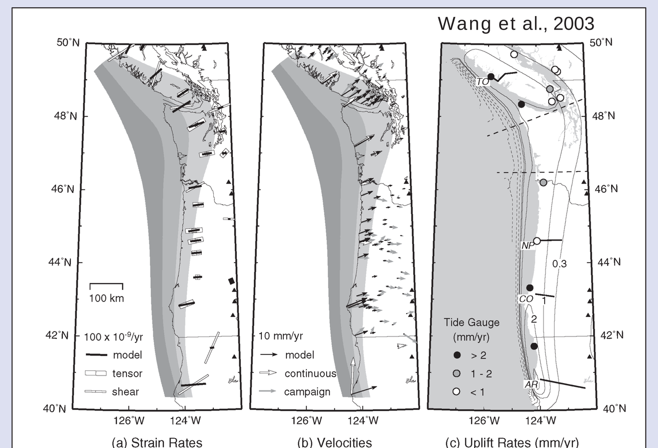

Model results of CAS3D-2; view of the locked zone (darkest shading) and ETZ of the Cascadia subduction fault at present assumed by CAS3D-2. ETZ is divided into two halves, and only the seaward half (intermediate shading) is involved in the calculation of potential coseismic deformation.Fault zone shading is the same as in Figure 10. (a) Model and observed strain rates. The ‘‘tensor’’ strain rates are the best geodetic data constraints for an interseismic deformation model. (b) Model velocities and GPS velocities. GPS data for central and southern Cascadia have been corrected for secular forearc motion (Figure 3). (c) Model uplift rates (contour lines) and uplift rates derived from tide gauge records.

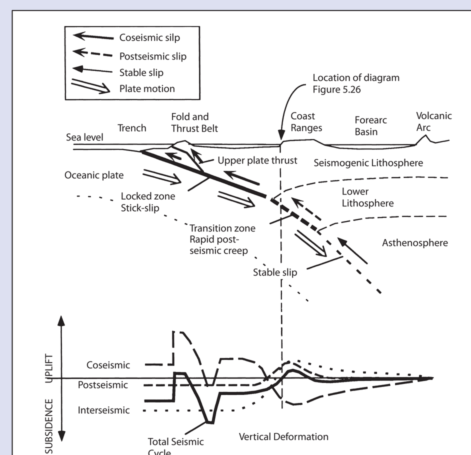

Pattern of deformation across a Chilean-type subduction zone (Plafker, 1972) for interseismic, coseismic, and postseismic parts of the seismic cycle. During the long duration interseismic part of the cycle, the locked zones of the megathrust are coupled and the upper plate is carried toward the arc and down with the descending oceanic plate. Compression of the backstop region above the transition zone and the deep stable sliding part of the megathrust generates uplift near the arc. During megathrust earthquakes, coseismic slip on the locked zone produces uplift above the megathrust rupture and elastic relaxation and subsidence between the downdip end of rupture and the arc. Slip on upper plate thrusts can generate localized and permanent uplift and subsidence in the fold and thrust belt. Rapid creep accommodates the slip deficit on the megathrust in the transition zone during the relatively short postseismic interval following the earthquake. This rapid creep produces rapid rebound in the area of coseismic subsidence.

McCalpin and Carver, 2009

Humboldt Bay:

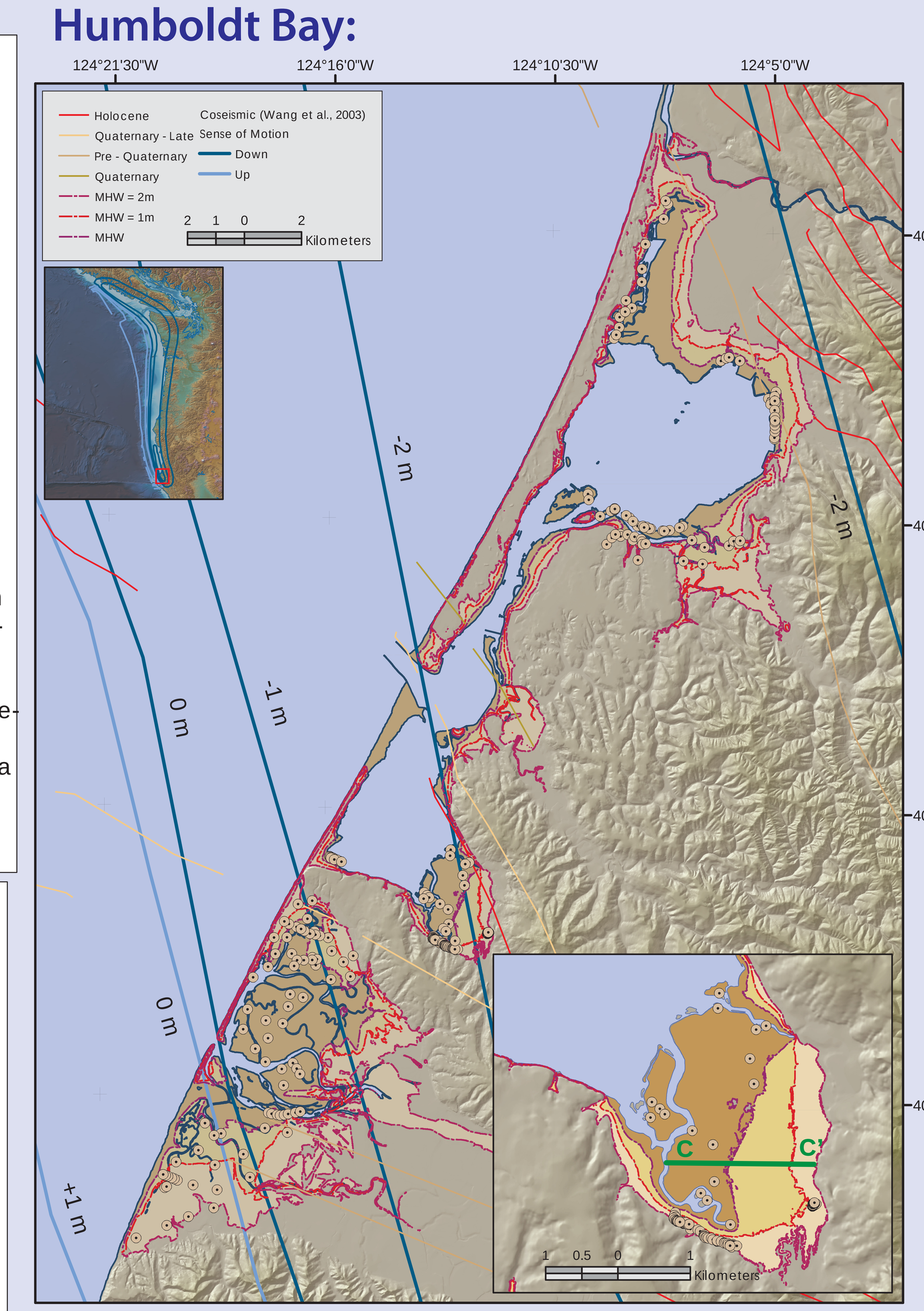

Geodesy:

Wang et al., 2003
Mitchell et al., 1994

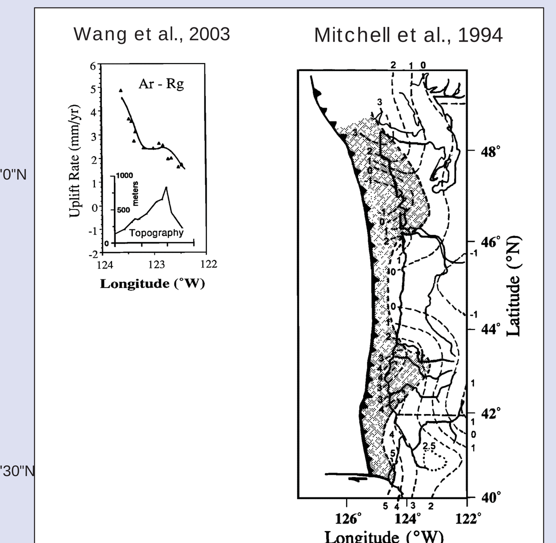

Mitchell et al., 1994

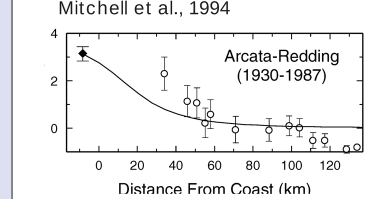

Upper left and bottom, east-west uplift rate profiles from Arcata to Redding based on releveling. The Arcata data point is actually ~30 miles east of Arcata, so is incorrectly labeled in these two papers (Mitchell et al, 1994; Wang et al., 2003).

On upper right is a contour map of present-day uplift rates for the CSZ. Contours are generated from tidal records and leveling profiles. The stippled area is an interpretation of the region of elastic strain accumulation, assuming that the most rapid uplift at the surface approximately overlies the downdip edge of the portion of the subduction zone interface.

Crescent City/North Spit Tide Gages

NOAA tide gage data from Crescent City and North Spit (Humboldt Bay). What can you conclude from these two data sets?

Assuming these locations are receiving the same global sea-level rise, tectonics might be invoked to explain the difference in these records.

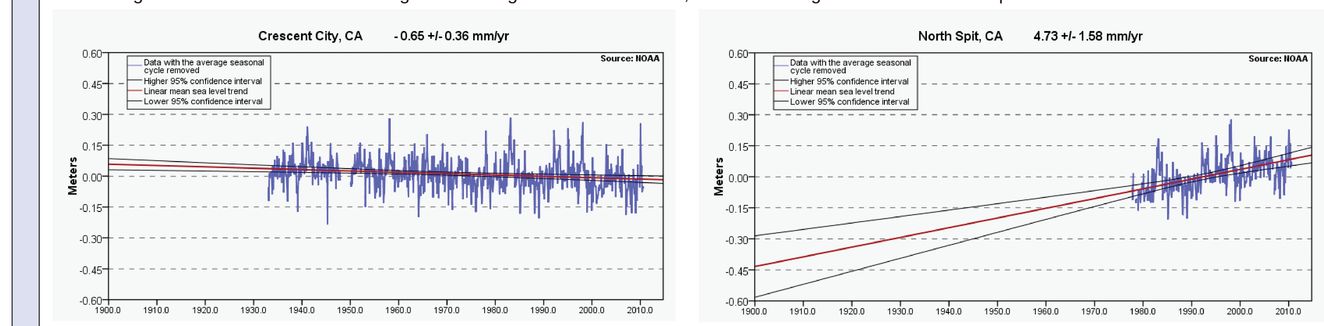

Mad River Slough Relative to North Spit

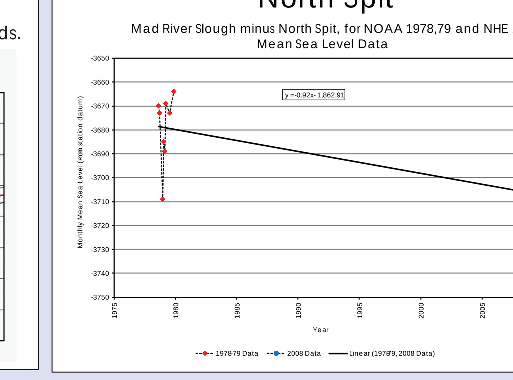

GPS

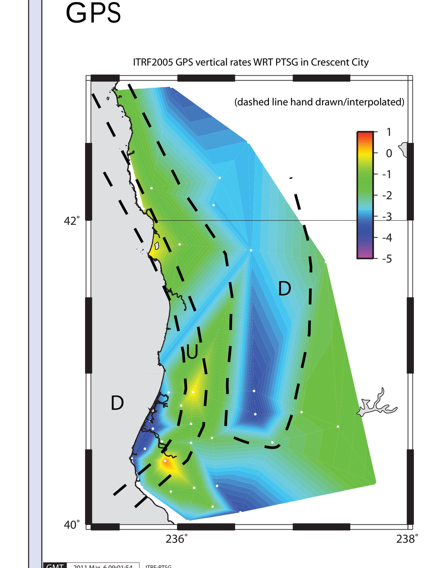

Global Positioning System (GPS) geodetic measurements of tectonic ground deformation in northern California. Dashed lines designate hand drawn countours of vertical movement for the time period during which these measurements were collected. D represents regions of interseismic subsidence and U represents regions of interseismic uplift. Remember, coseismic deformatin is probably the opposite sense of motion.

Paleogeodesy

Leonard et al., 2009

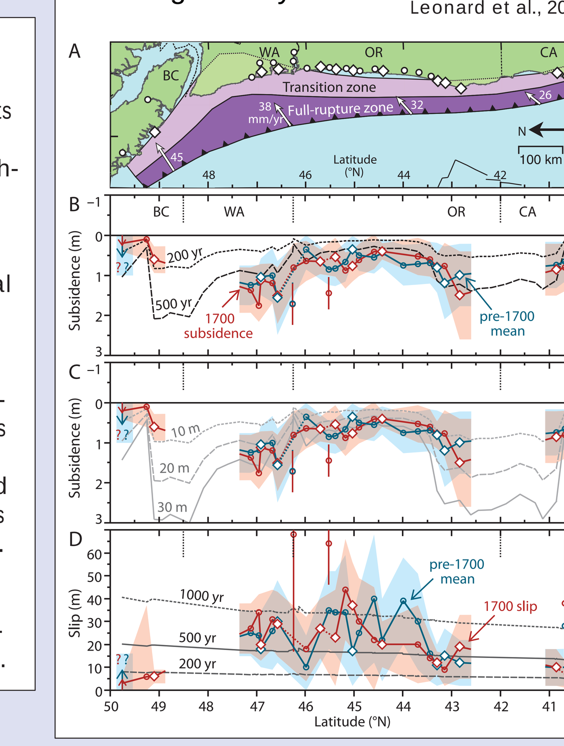

Comparison of coseismic subsidence and megathrust slip among the A.D. 1700 earthquake (T1), previous recorded events (averaged), and the predictions of elastic dislocation models. (A) Averaged locations of coastal coseismic subsidence sites relative to the full-rupture (purple) and transition (lilac) zones. White diamonds and circles—sites with high- and low-quality subsidence estimates, respectively. See Figure 3 for site names. White arrows—plate convergence vectors. (B) Coseismic subsidence estimated at the above buried soil sites for the A.D. 1700 earthquake (red symbols and shading—weighted mean and uncertainty) and for pre–A.D. 1700 recorded events (blue symbols and shading—mean and uncertainty). Upward/downward arrows with question marks indicate unquantifi able estimates of uplift/subsidence. Two low-quality data points are excluded from the shading as they appear to be outliers; these include data from the Columbia River that are questionable due to possible freshwater influence (Leonard et al., 2004). Dashed darkgray lines show coseismic subsidence predicted by the elastic dislocation model at the same sites for the release of 200 and 500 yr of accumulated strain. (C) As in B, except the gray lines represent coseismic subsidence predicted for uniform megathrust slip of 10, 20, and 30 m. (D) Along-strike megathrust slip variations estimated for the A.D. 1700 (red symbols and shading—weighted mean and uncertainty) and previous events (blue symbols and shading—mean and uncertainty) from the correspondence between observed coseismic subsidence and that predicted from uniform slip models (C). Dark-gray lines show the along-margin slip pattern expected for the release of 200, 500, and 1000 yr of accumulated strain.

Mechanisms likely responsible for this mismatch include (1) upper plate fault rupture (e.g. Patton Bay fault in 1964 Alaska)(2) varying land-level / sea-level relations during coseismic periods, (3)spatial variation in slip patches along the megathrust for different earthquakes, (4) and deep locking and deep slip on the megathrust (similar to 2011 Tohoku-Oki). Tide gage deployments in the next year and updates to level surveys around Humboldt Bay will help reveal more details about the spatial variation in fault coupling. Resampling buried soils for new AMS radiocarbon ages will also provide more details that might further reveal age discordance in regions affected by different upper plate faults of the accretionary prism in northern California.

Possible Causes for mismatch:

Upper Plate Earthquakes

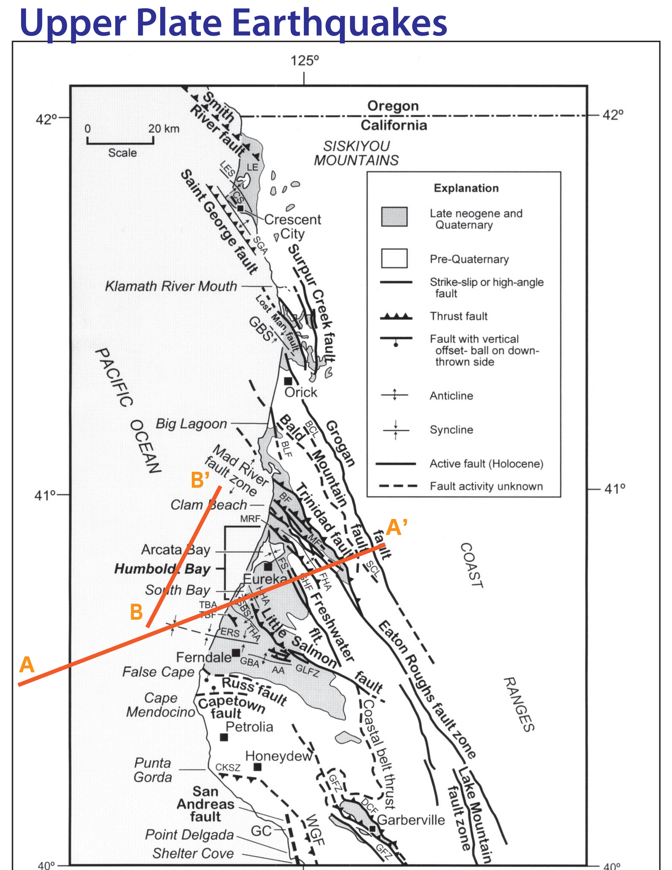

Kelsey, H.M., 2001, Active faulting associated with the southern Cascadia subduction zone in northern California, Ferriz, H. and Anderson, R. (eds), Engineering Geology Practice in Northern California, Division of Mines and Geology Bulletin 210, Association of Engineering Geologists Special Publication 12, p. 259-274.

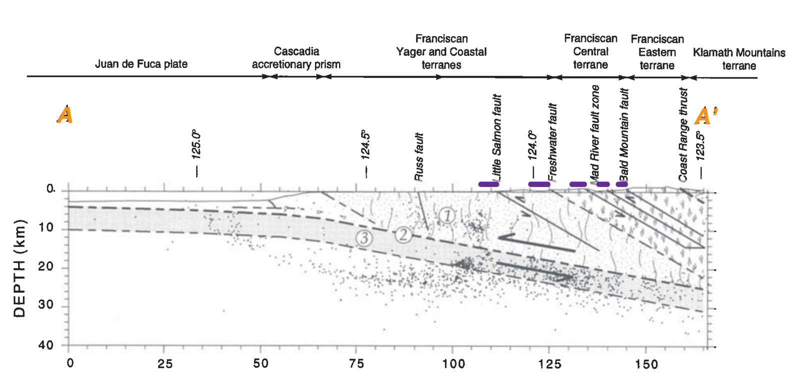

Figure 1b. Generalized east-west cross section across the southern Cascadia subduction margin showing inferred configuration of major basement units at no vertical exaggeration, location of crustal structures, and location of potential seismic sources (modified from *McCrory* [1996a]). See Figure 1a for location of Profile AA'. 1, upper plate, northern California crustal sources; 2, interplate megathrust sources; 3, lower plate, Juan de Fuca sources. Dots denote ambient seismicity ca. 1975-1996 in a 20 km swath centered on the profile line (D. H Oppenheimer, unpublished data, 1996). The location of the Juan de Fuca plate beneath the margin is constrained by these earthquake hypocenters. Arrows denote relative movement on Cascadia megathrust and Little Salmon and Mad River fault zones. Plot suggests that some ambient crustal seismicity may correlate with mapped Quaternary thrust faults in Franciscan rocks. The patterns used to denote basement units are the same for Figures 1a, 2, and 4.

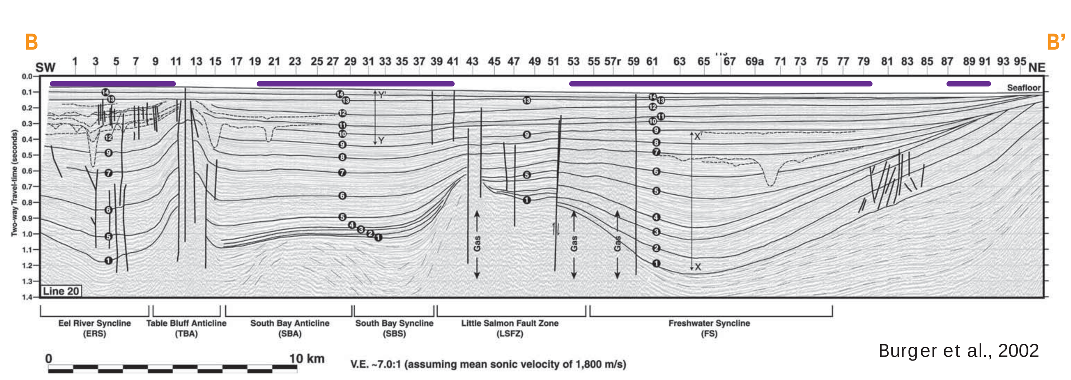

Burger et al., 2002

Interpreted versions of seismic strike profile B-B', showing mapped faults, deformational structures, and unconformities (numbered circles). Near-vertical bold lines represent faults, solid lines represent regional unconformities, dashed lines represent local incised unconformities, and fine dashed lines represent the trends of folded and truncated reflectors beneath surface 1. Vertical zones of presumed gas wipeout (Yun et al., 1999) are present within the TBA and the LSFZ. Lateral extents of onshore structures mapped onshore are indicated at the bottom of the interpreted profile.

RSL/RLL Relations

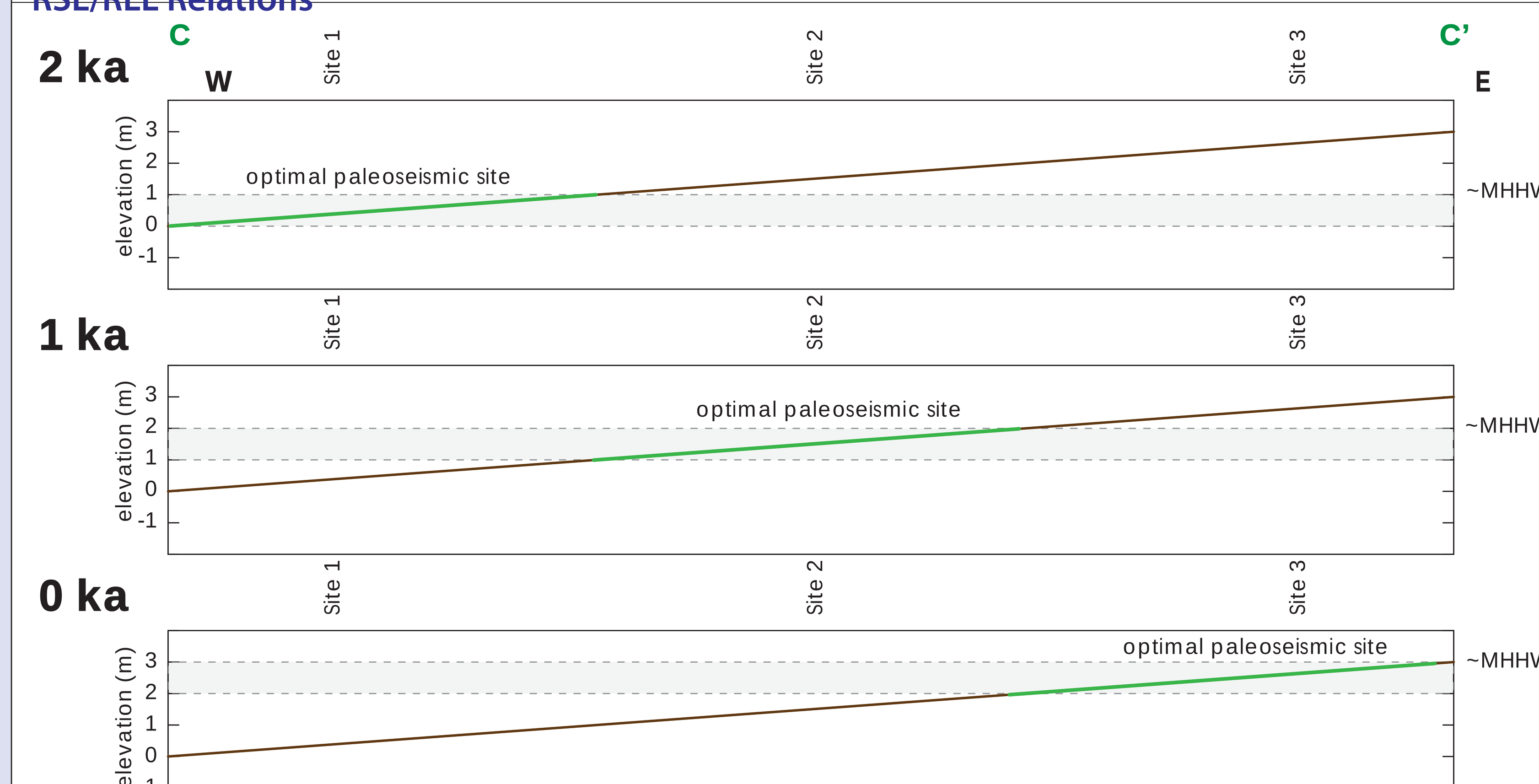

Three periods in time with rising sea-level of 1 mm/yr. on westward tilting ground surface, the optimal paleoseismic sites migreate eastward. Optimal paleoseismic sites are regions that are more likely to record a contrast in litho- and bio-stratigraphy following an earthquake. These regions, in green, are vertically restricted to the higher tidal elevations.

Nelson et al., 2006

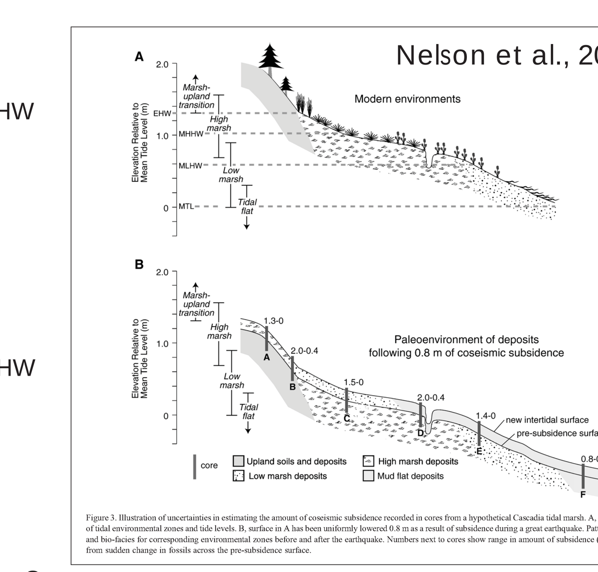

Figure 3. Illustration of uncertainties in estimating the amount of coseismic subsidence recorded in cores from a hypothetical Cascadia tidal marsh. A, elevation ranges of tidal environmental zones and tide levels. B, surface in A has been uniformly lowered 0.8 m as a result of subsidence during a great earthquake. Patterns show litho- and bio-facies for corresponding environmental zones before and after the earthquake. Numbers next to cores show range in amount of subsidence (meters) inferred from sudden change in fossils across the pre-subsidence surface.

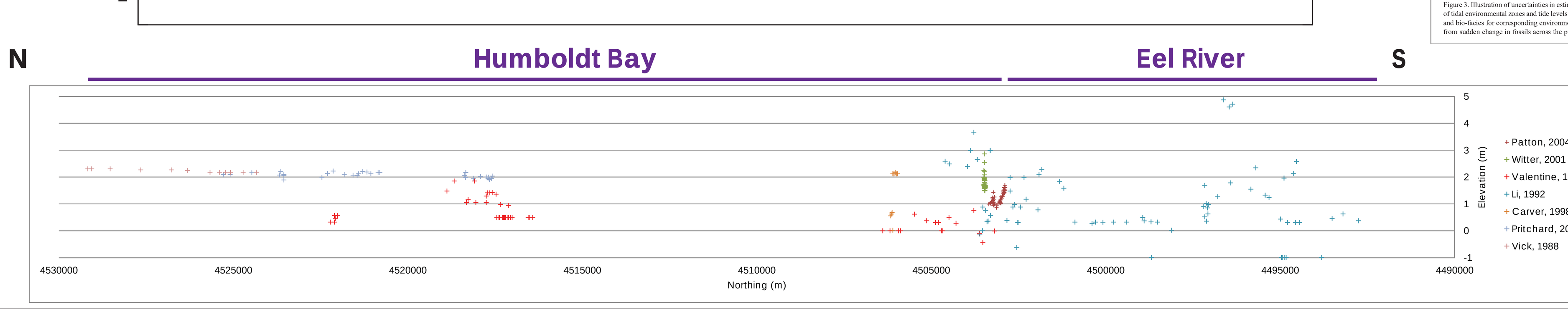

Ground surface elevations are plotted for cores collected for paleoseismic and paleotsunami investigations around Humboldt Bay and the Eel River delta. Older core elevations are based on 10m DEM elevations. Modern studies rely on total station surveys to the nearest tidal benchmarks. The vertical datum for all cores is NAVD88.

Temporal Variation in Slip Distribution

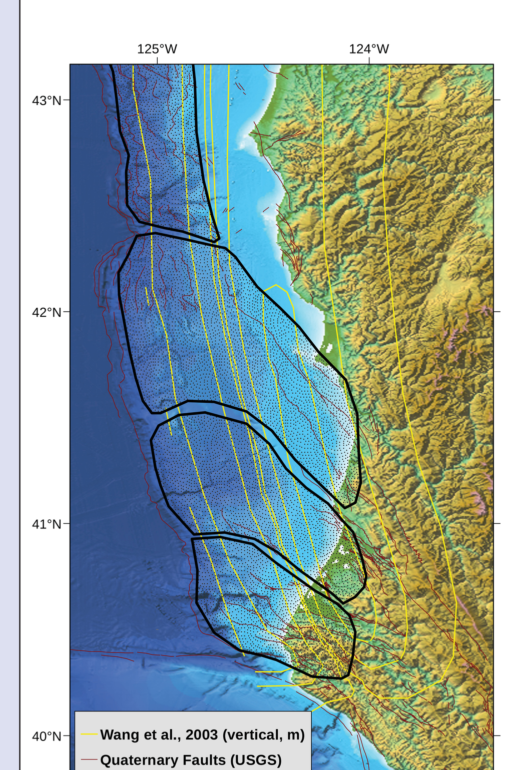

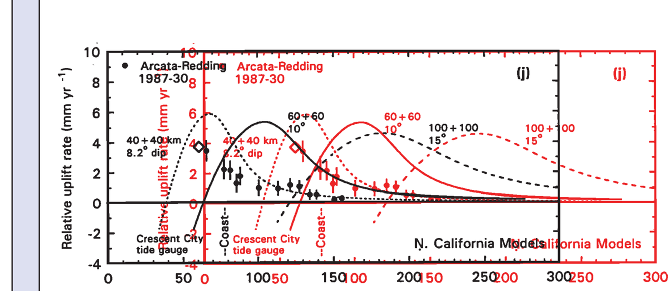

Hyndman and Wang, 1995

Loveless and Meade, 2010

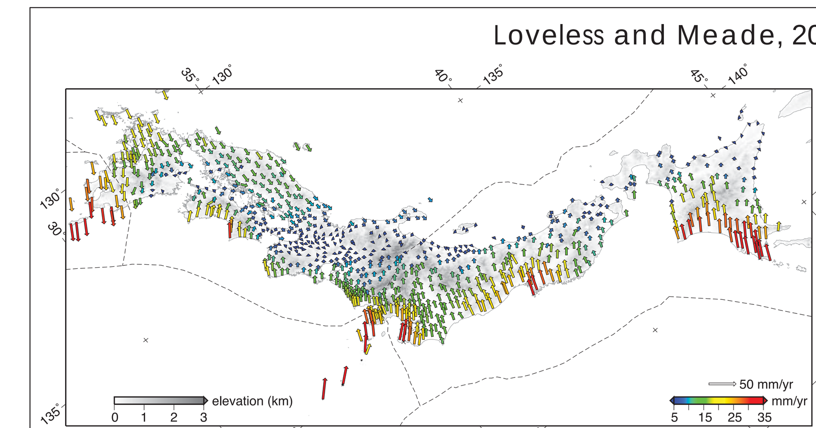

Nominally interseismic GPS velocity field in Japan derived from GEONET data between 1997 and 2000, expressed in a stable Eurasian reference frame [Apel et al., 2006]. Velocity magnitude is indicated both by vector length and color. Dashed lines show plate boundaries from Bird [2003].

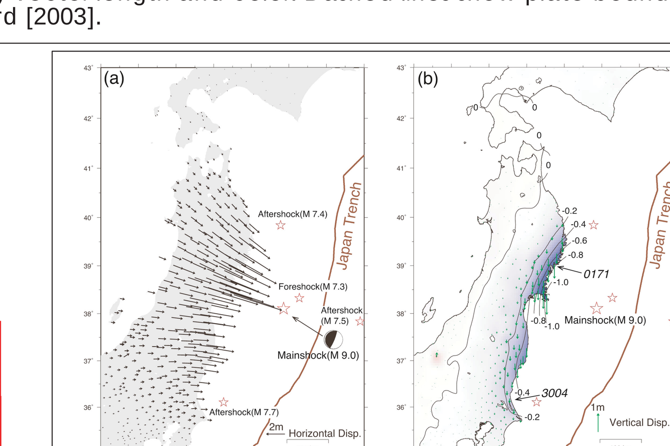

Coseismic displacement of the 2011 Tohoku earthquake based on daily coordinates of the routine GEONET analysis. (a) Horizontal displacement. The focal mechanism of the mainshock is from the Global CMT Project (http://www.globalcmt.org/). (b) Vertical displacement.

Nishimura et al., 2011